ELSEVIER

International Journal of Heat and Fluid Flow 23 (2002) 657–663

International Journal of HEAT AND FLUID FLOW

www.elsevier.com/locate/ijhff

Instability in three-dimensional, unsteady, stenotic flows

Francois Mallinger, Dimitris Drikakis *

Engineering Department, Queen Mary, University of London, London E1 4NS, UK

Abstract

The paper presents a computational investigation of instabilities in pulsatile flow through a three-dimensional stenosis. The computations have been conducted using a third-order high-resolution scheme and a non-linear multigrid algorithm. The simulations reveal the existence of unstable flow throughout the pulsatile cycle. The instability is manifested by asymmetric flow patterns—though the stenosis is axisymmetric—large flow variations in the cross-sectional planes, and swirling motion in the poststenotic region. The instability leads to a strongly disturbed flow several radii downstream of the stenosis, as well as spatio-temporal fluctuations of the circumferential shear stress and vorticity.

1. Introduction

In the context of biofluid mechanics, the computational study of flows through stenoses is motivated by the need to obtain a better understanding of the impact of flow phenomena on diseases such as atherosclerosis and stroke. The flow phenomena occurring in stenotic arteries include asymmetric flow separation, instabilities and laminar-to-turbulent transition. These phenomena may have significant effects on the wall shear stress (WSS). Past experimental studies have shown that in pulsatile flows both high and low WSS values have important haemodynamic effects (Ku et al., 1985; Caro et al., 1971); the former because of their magnitude and the latter because of their rapid variations in space and time. A review of past experimental and theoretical studies is given in Berger and Lou (2000).

A better understanding of flows through stenosis may also contribute to improvements in medical diagnosis procedures and stenosis-detection techniques. By analyzing the noise generated by a poststenotic disturbed flow it may be possible to localize artery constriction. Experiments have been performed by Clark (1980) aiming at analyzing turbulence produced by stenosis. Khalifa and Giddens (1981) have also conducted similar experiments aiming at relating the level of disturbances of the poststenotic flow to the degree of stenotic obstruction. However, the flow through a stenosis is far from being well understood.

To our knowledge, a computational study of three-dimensional, pulsatile and unstable flow through a stenosis has not previously been conducted. Previous computational studies were concerned with steady and unsteady axisymmetric flows; for example, see the recent study by Stroud et al. (2000) in which a numerical investigation of the flow in stenotic axisymmetric vessels of different shapes was presented. In the present paper, we study by means of numerical simulations pulsatile, three-dimensional, unstable flow through a stenosis and examine the effects of the instability on the wall shear-stress, velocity and vorticity fields.

The paper is organised as follows. The flow problem and numerical procedure is described in Section 2. The onset of the instability is discussed in Section 3. In Sections 4 and 5, we discuss the effects of the instability on the WSS and vorticity generation, respectively. Finally, Section 6 summarises the conclusions drawn from the present investigation.

2. Problem description

The stenosis model considered here is similar to the one used by Khalifa and Giddens (1981) in their experimental study. These experiments do not provide

* Corresponding author. Tel.: +44-20-78825194; fax: +44-20-89831007.

E-mail address: d.drikakis@qmul.ac.uk (D. Drikakis).

0142-727X/02/$ - see front matter
PII: S0142-727X(02)00161-3

Nomenclature

D	diameter of the pipe
f_u, f_v, f_w	white-noise perturbation functions associated with the inlet $u_{\text{in}}, v_{\text{in}}$ and w_{in} velocity components, respectively.
u_{a}	amplitude of the sine-wave velocity
u, v, w	Velocity components
u_{m}	temporal mean centreline velocity at the inlet
R	radius of the pipe
v	kinematic viscosity
$Re = u_{\text{m}}R/v$	Reynolds number
r	radial position with origin the pipe centre
t	time
x	Cartesian co-ordinate in the streamwise direction
y, z	Cartesian co-ordinates in the cross-sectional plane
ω	frequency
ω_x	streamwise vorticity
$\alpha = R(\omega/v)^{1/2}$	Womersley number
τ_{xn}	longitudinal wall shear stress
τ_{tn}	circumferential wall shear stress

sufficient information for validating CFD models, but they have demonstrated that stenotic pulsatile flows are indeed associated with flow disturbances phenomena and large-scale structures, which deviate from the laminar flow behaviour.

The geometry consists of an axisymmetric stenosis with 75% reduction in the cross-sectional area, i.e., the stenotic area is 25% of the pipe area (Fig. 1). We have conducted several numerical experiments using different pipe lengths upstream and downstream of the stenosis in order to ensure independence of the results from the position of the inflow and outflow boundaries. We have found that $2D$ and $70D$ lengths upstream and downstream, respectively, are sufficient. Time-dependent, three-dimensional flow computations were carried out on a grid containing 250,000 ($400 \times 25 \times 25$) cells; the grid was non-uniform in the radial direction with a clustering of grid lines in the near wall region. Note that in the literature simulations of stenotic flows using even coarser grids have been reported (Berger and Lou, 2000; Stroud et al., 2000). In a recent simulation study of arterial flows (Prakash and Ethier, 2001), it was shown that 325,000 grid nodes are required to achieve grid independence in the WSS field and about 190,000 nodes to achieve less than 10% spatial discretisation error in the WSS. Although we do not claim that the grid employed here provides a grid independent solution in the WSS field, we have found that the flow remains (at least) qualitatively the same on an even coarser grid containing about 150,000 cells; the difference in averaged WSS when changing from 150,000 to 250,000 cells is about 9%. Since our objective is to qualitatively study the unstable flow, the grid containing 250,000 cells can be considered as a good compromise between accuracy and computational cost.

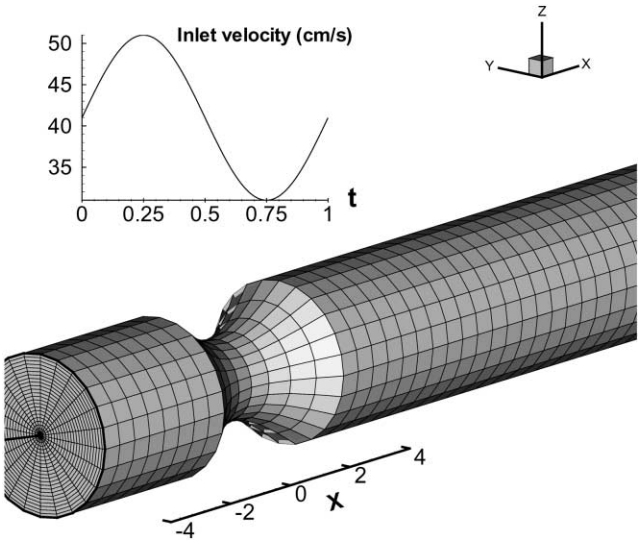

Fig. 1. The inlet velocity profile (top) and stenosis geometry (bottom) used in the computations; the unit is the radius of the pipe R. The stenosis length is $4R$.

The inlet streamwise velocities $u_{\text{in}}(y, z, t)$ was defined by a perturbed parabolic profile

$$u_{\text{in}}(y, z, t) = [u_{\text{m}} + u_{\text{a}} \sin(\omega t) + f_u(y, z, t)]\left[1 - \frac{y^2 + z^2}{R^2}\right], \tag{1}$$

where the inlet centreline velocity is given by the sum of a mean velocity $u_{\text{m}} = 41$ cm/s, and a sine-wave of frequency $\omega = 2\pi$ and amplitude $u_{\text{a}} = 10$ cm/s (Fig. 1). The function $f(y, z, t)$ is a time-dependent white-noise perturbation with amplitude 20% of u_{m}.

The inlet velocities $v_{\text{in}}(y, z, t)$ and $w_{\text{in}}(y, z, t)$ were also defined by a formula similar to (1) with $u_{\text{m}} = u_{\text{a}} = 0$ and amplitude of perturbations 15% of u_{m}

$$v_{\text{in}}(y, z, t) = f_v(y, z, t)\left[1 - \frac{y^2 + z^2}{R^2}\right], \tag{2}$$

$$w_{\text{in}}(y, z, t) = f_w(y, z, t)\left[1 - \frac{y^2 + z^2}{R^2}\right]. \tag{3}$$

Numerical experiments showed that a further increase in the magnitude of the initial perturbations did not change (at least qualitatively) the flow results. [1]

No-slip boundary conditions were used on the walls of the pipe. At the outlet the second-order derivatives of the flow variables were set equal to zero. The instantaneous Reynolds number, based on the centreline temporally averaged streamwise velocity and the pipe radius, has minimum and maximum values of 760 and 1245, respectively. The pulsatile frequency number (Womersley number) is $\alpha = 9.87$. The above values of Reynolds and Womersley numbers are within the range of values found in animal experiments (Giddens et al., 1976); similar values were also used by Khalifa and Giddens (1981) in their laboratory experiments.

The computational investigation is based on the three-dimensional Navier–Stokes equations for an incompressible fluid. We have assumed the fluid to be Newtonian, a generally accepted approximation of the rheological behaviour of blood in the larger blood vessels. Additionally, we have considered the arterial wall to be rigid. The above two assumptions are introduced in order to simplify the analysis of our simulations and thus develop a gradual understanding of the unstable flow through a stenosis. The computational code employs the finite volume approach and curvilinear co-ordinates. The numerical algorithm is based on high-resolution third-order schemes (Drikakis, 2001) and a non-linear multigrid method (Drikakis et al., 1998) in conjunction with a TVD fourth-order Runge–Kutta scheme (Shu and Osher, 1988) for the time integration. The continuity and momentum equations are solved in a coupled fashion using dual-time stepping (Merkle and Athavale, 1987; Rogers et al., 1991) in conjunction with the artificial-compressibility approach (Chorin, 1967). The present method allows large time steps to be employed without degrading the stability of the numerical solution. Further details about the numerical method can be found in Drikakis et al. (1994, 1998, 2001). Validation of the computer code for flows relevant to the one discussed here has been presented in various past papers (Drikakis et al., 1994; Drikakis and Papadopoulos, 1996; Drikakis, 1996, 1997).

3. Onset of instability

In the numerical simulation the onset of instability can be detected as asymmetric flow in the cross-sectional planes. The instability results in substantial asymmetries within the separated flow region downstream of the stenosis. Note that in the case of stable flow the solution will remain axisymmetric throughout the domain, even when random perturbations are imposed on the initial velocity profiles. In this case, the axisymmetry of the flow will be established after a few pulsatile cycles.

The flow instability through a stenosis resembles flow instabilities occurring in flows through a sudden expansion. The phenomenon of asymmetric separation in suddenly expanded (steady) flows has been discussed in several previous experimental (Chedron et al., 1978; Fearn et al., 1990) and computational (Alleborn et al., 1997; Drikakis, 1997) works. The above studies have shown that at very low Reynolds numbers suddenly expanded flows remain symmetric, but with increasing Reynolds number flow asymmetries begin to appear.

Here, computations were carried out for several pulsatile cycles until the instability was fully established. Nine to eleven cycles were found sufficient for obtaining a full spatial growth of the instability. In qualitative terms the flow evolves in a similar fashion across different pulsatile cycles after the instability is established. The instability initiates inside the stenosis and fully establishes downstream of it. In Fig. 2, asymmetric flow patterns in different cross-sections downstream of the stenosis are shown by means of isocontour plots of the streamwise velocity. The breaking of the flow symmetry is associated with the formation of a vortex on the upper part of the cross-section (see plots for $x = 2.5$ in Fig. 2).

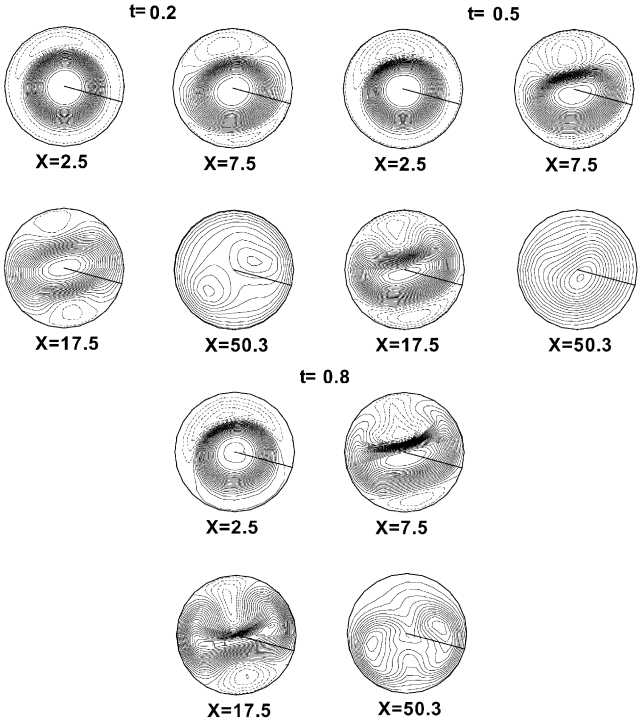

Fig. 2. Isocontours of the streamwise velocity at different time instants and cross-sections.

[1] There is a threshold value for the forcing amplitude due to numerical considerations. We have found that if the forcing amplitude is sufficient small the perturbations will be attenuated quickly due to numerical dissipation; this also depends on the properties of the numerical scheme employed (Drikakis and Smolarkiewicz, 2001).

As the instability spreads downstream a second vortex occurs on the lower part of the cross-section (see plots for $x = 7.5$). The vortices emerge from the near-wall region and gradually occupy a large part of the cross-sectional area. Previous experiments (Chedron et al., 1978; Fearn et al., 1990) and simulations (Drikakis, 1997) of suddenly expanded channel flows have shown that at relatively low Reynolds numbers the instability appears near the expansion as asymmetric separation on the upper and lower channel walls without the presence of three-dimensional effects. In the present case, the breaking of the flow axisymmetry is associated with changes in both the longitudinal and circumferential direction, but the intensity of asymmetries in the secondary plane readily increases further downstream (for example, at $x = 50.3$). The asymmetric flow behaviour persists over a few radii downstream prior to the flow becoming fully axisymmetric again.

With respect to the spatial growth of the instability, the simulations revealed that important flow changes occur within two downstream regions. These can be observed in the isosurfaces of the streamwise velocity at different time instants (Fig. 3). The first region (labelled "region A") is closer to the constriction and encompasses the fluid jet arising from the stenotic region. In the region A, the instability has been established, but has not broken the coherence of the fluid jet. The second region (labelled "region B") is further downstream where substantial variations of the flowfield occur. In this region, the coherence of the fluid jet cannot be maintained due to the swirling motion of the fluid. Although the lengths of the regions A and B vary among different time instants, the largest flow variations take place within $x = 30$–50 radii downstream of the stenosis.

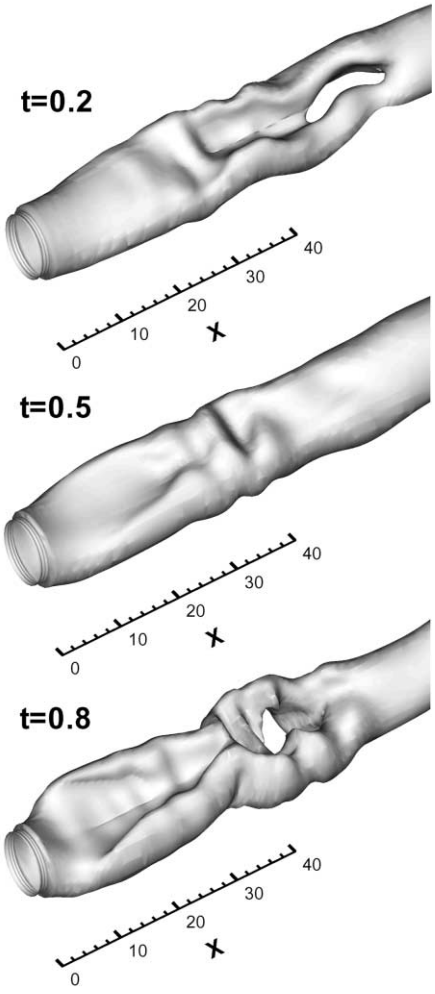

Fig. 3. Isosurfaces of the streamwise velocity at different time instants: $u = 0.96$ at $t = 0.2$; $u = 0.66$ at $t = 0.5$; and $u = 0.62$ at $t = 0.8$.

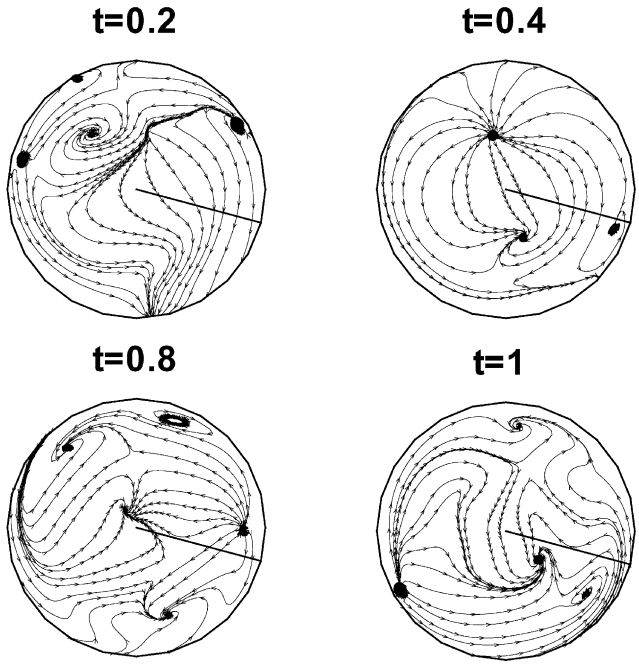

Fig. 4. Cross-flow streamtraces of the velocity field at different time instants for $x = 30$.

Fig. 4 shows the cross-flow streamtraces of the velocity field at different time instants for the cross-section at $x = 30$. As a result of the instability, the critical points (points of zero velocity) vary in number and location at different time instants.

4. Wall shear stress

Fig. 5 shows isocontours of the longitudinal component, τ_{xn}, of the wall shear-stress at five different time instants; τ_{xn} is calculated by projecting the velocity vector onto a direction tangent to the wall, facing the streamwise direction. The separated flow region, indicated by negative shear stress, is extended up to 60 radii ($t = 0.8$) downstream of the stenosis (Fig. 5). The extent

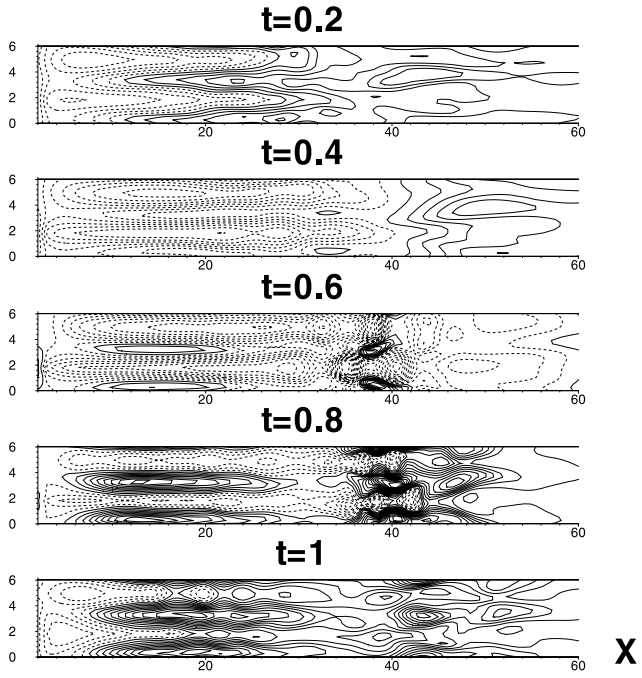

Fig. 5. Isocontours of τ_{xn} at different time instants; dashed and solid lines denote negative and positive stresses, respectively.

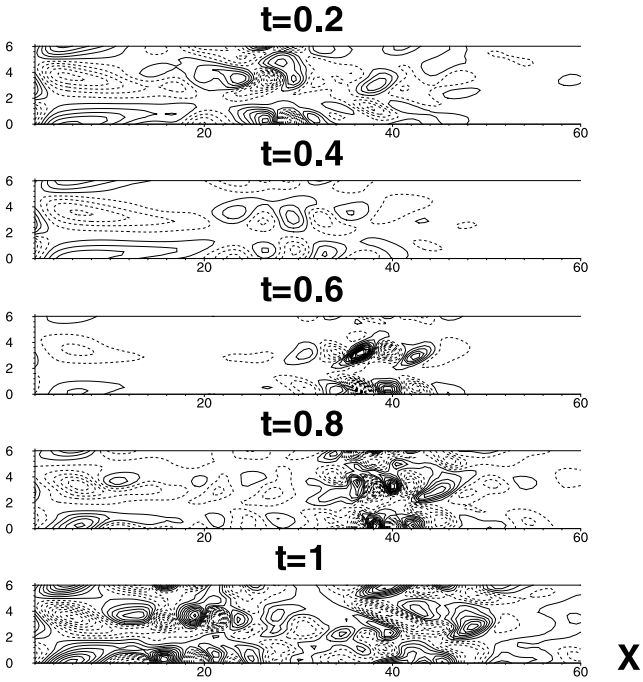

Fig. 7. Isocontours of τ_{tn} at different time instants.

of separation is reduced at the beginning of the pulsatile cycle.

Furthermore, in the region A we observe elongated structures emerging from the exit of the stenosis. These elongated structures are due to the distortion of the fluid jet from an axisymmetric profile as a result of the two vortices emerging from the near wall region (Fig. 2). The distortion of the fluid jet also leads to the formation of "bubbles" (Fig. 5 for $t = 0.6$–0.8) of positive wall shear-stress, inside the regions of negative stresses. Strong mixing of positive and negative stresses occurs between $x = 35$ and 45. For all time instants the largest values of τ_{xn} appear in the stenotic region (Fig. 6). The peak value occurs at the centre of the stenosis.

In Fig. 7, the isocontours of the circumferential component of the shear stress τ_{tn} are shown; τ_{tn} is calculated by projecting the velocity vector onto a direction tangent to the wall, orthogonal to the streamwise

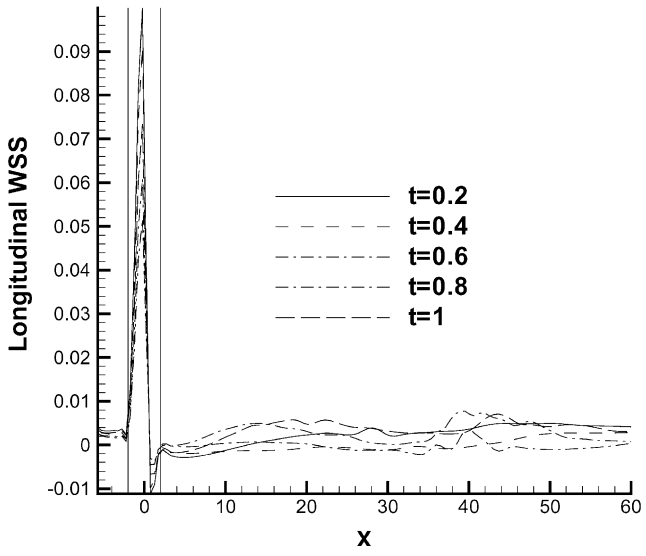

Fig. 6. Distribution of maximum τ_{xn} (for each cross-section) at five different time instants. The two vertical lines represent the beginning and end of the stenosis.

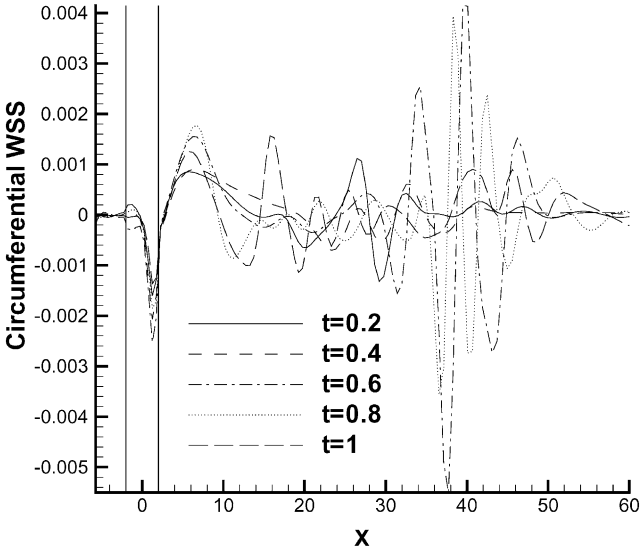

Fig. 8. Distribution of maximum τ_{tn} (for each cross-section) at five different time instants. The two vertical lines represent the beginning and end of the stenosis.

direction. Similar to τ_{xn}, elongated structures of τ_{tn} appear close to the constriction region, but they extend to a smaller area compared to τ_{xn}. Another observation is that the mixing of regions of positive and negative stresses is more evident for τ_{tn} than τ_{xn}. The maximum values of τ_{tn} at each cross-section are plotted in Fig. 8. The results show that τ_{tn} is significantly smaller, as expected, than τ_{xn} in the region of the stenosis. On the other hand, substantial variations of τ_{tn} occur in the region B with the peak value of τ_{tn} occurring at $x = 40$ (Fig. 8). This is in accord with the results discussed in the previous section concerning the breaking of flow coherence and swirling motion in the region B.

5. Vorticity

Fig. 9 shows the zero isosurface of the streamwise vorticity, ω_x, as well as volumes of positive (gray) and negative (black) streamwise vorticity at $t = 0.4$. In the region A the surface consists of a superposition of elongated vorticity sheets. Further downstream, these sheets roll up to form conical structures facing the streamwise direction. Elongated "half-ring" like structures, formed by positive and negative vorticity, arise from the exit of the stenosis and terminate at about $x = 21$ (Fig. 9). Further downstream, these structures break up into smaller ones because of the full development of the three-dimensional instability. In the region B, positive and negative vorticity regions alternate in both the streamwise and radial directions.

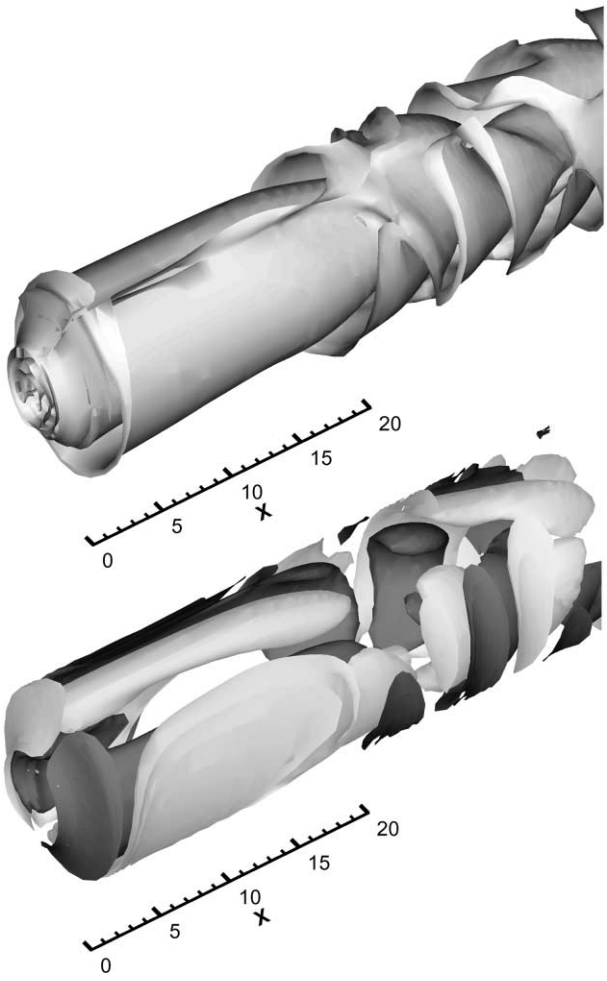

Fig. 9. Zero isosurface of the streamwise vorticity ω_x at $t = 0.4$ (top) and volumes of positive (gray) and negative (black) streamwise vorticity ω_x at $t = 0.4$ (bottom).

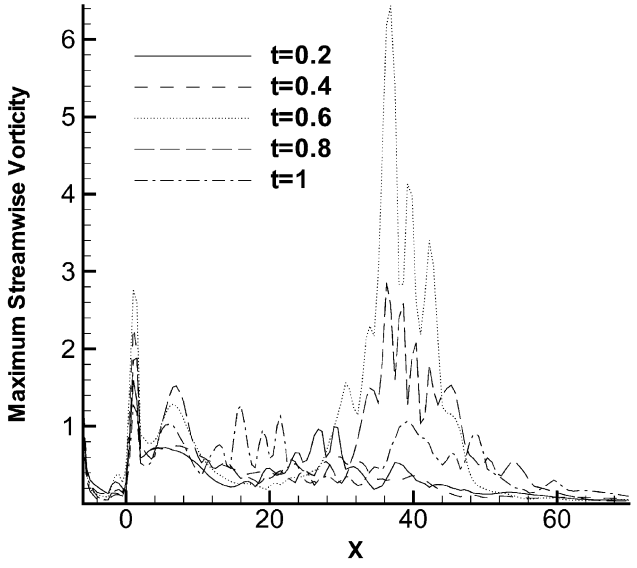

Fig. 10. Distribution of the maximum (per cross-section) value of the vorticity component ω_x at different time instants.

The longitudinal distribution of the maximum (per cross-section) value of the vorticity component ω_x at different time instants is shown in Fig. 10. The vorticity exhibits large variations in the region B during the deceleration phase of the flow. This is in accord with our previous observation that intense swirling of the flow occurs in this region. Moreover, ω_x exhibits a peak value in the stenosis where the onset of instability takes place.

6. Concluding remarks

Numerical simulation of pulsatile flow through a symmetric stenosis revealed a three-dimensional instability with profound effects on the flow development. The simulation showed that most of the important flow changes concentrate in two poststenotic regions. In the first region, closer to the constriction, the instability is primarily associated with streamwise flow changes. In this region the coherence of the fluid jet, arising from the stenosis, is maintained until the second poststenotic region begins. In the second region the flow exhibits

swirling and the coherence of the fluid jet cannot be maintained. These effects are also associated with an increase of the circumferential stress, as well as large spatial and temporal fluctuations of the WSS and vorticity.

In the context of medical diagnosis, it is important to detect as accurately as possible the size and location of the artery obstruction. The present results show that due to the flow instability important variations occur after the stenosis. Subsequently, this flow behaviour may need to be taken into account by diagnostic criteria and detection techniques used in clinical practice.

Acknowledgements

The financial support from EPSRC (GR/L71568) is gratefully acknowledged. We would also like to thank M. Leschziner and the anonymous reviewers for their comments on the manuscript.

References

Alleborn, N., Nandakumar, K., Raszillier, H., Durst, F., 1997. Further contributions on the two-dimensional flow in a sudden expansion. J. Fluid Mech. 330, 169–188.

Berger, S.A., Lou, L.-D., 2000. Flows in stenotic vessels. Ann. Rev. Fluid Mech. 32, 347–382.

Caro, C.G., Fitzgerald, J.M., Schroter, R.C., 1971. Atheroma and arterial wall shear observations, correlation and proposal of a shear dependent mass transfer mechanism for artherogenesis. Proc. Roy. Soc. Lond. Ser. B 17 (7), 109–159.

Chorin, A.J., 1967. A numerical method for solving incompressible viscous flow problems. J. Computat. Phys. 2, 12–26.

Chedron, W., Durst, F., Whitelaw, J.H., 1978. Asymmetric flows and instabilities in symmetric ducts with sudden expansion. J. Fluid Mech. 84, 13–31.

Clark, C., 1980. The propagation of turbulence produced by a stenosis. J. Biomechan. 13, 591–604.

Drikakis, D., 1996. A parallel multiblock characteristics-based method for 3D incompressible flows. Adv. Eng. Software 26, 111–119.

Drikakis, D., 1997. Study of bifurcation flow phenomena in incompressible sudden-expansion flows. Phys. Fluids 9 (1), 76–87.

Drikakis, D., 2001. Uniformly high-order methods for unsteady incompressible flows. In: Toro, E.F. (Ed.), Godunov Methods: Theory and Applications. Kluwer Academic Publishers, 263–283.

Drikakis, D., Papadopoulos, G., 1996. Experimental and numerical investigation of laminar-to-transitional pipe flow past a sudden expansion. In: Proceedings of the 1996 ASME Fluids Eng. Division, Summer Meeting, San Diego, California, July 7–11, vol. 2, pp. 679–684.

Drikakis, D., Smolarkiewicz, P.K., 2001. On spurious vortical structures. J. Computat. Phys. 172, 309–325.

Drikakis, D., Govatsos, P., Papantonis, D., 1994. A characteristic based method for incompressible flows. Int. J. Numer. Meth. Fluids 19, 667–685.

Drikakis, D., Iliev, O., Vassileva, D.P., 1998. A non-linear full multigrid method for the three-dimensional incompressible Navier–Stokes equations. J. Computat. Phys. 146, 301–321.

Fearn, R.M., Mullin, T., Cliffe, K.A., 1990. Nonlinear flow phenomena in a symmetric sudden expansion. J. Fluid Mech. 211, 595–608.

Giddens, D.P., Mabon, R.F., Cassanova, R.A., 1976. Measurements of disordered flow distal to subtotal vascular stenoses in the thoracic aortas of dogs. Circular Res. 39, 112–119.

Khalifa, A.M.A., Giddens, D.P., 1981. Characterization and evolution of poststenotic flow disturbances. J. Biomechan. 14 (5), 279–296.

Ku, D.N., Giddens, D.P., Downing, J.M., 1985. Pulsatile flow and atherosclerosis in the humna carotid bifurcation. Arteriosclerosis 5 (3), 293–302.

Merkle, C.L., Athavale, M., 1987. Time-accurate unsteady incompressible flow algorithms based on artificial compressibility. AIAA Paper, 87–1137.

Prakash, S., Ethier, C.R., 2001. Requirements for mesh resolution in 3D computational hemodynamics. J. Biomech. Eng. 123, 134–144.

Rogers, S.E., Kwak, D., Kiris, C., 1991. Steady and unsteady solutions of the incompressible Navier–Stokes equations. AIAA J. 29 (4), 603–610.

Shu, C.-W., Osher, S., 1988. Efficient implementation of essentially non-oscillatory shock-capturing schemes. J. Computat. Phys. 77, 439–471.

Stroud, J.S., Berger, S.A., Saloner, D., 2000. Influence of stenosis morphology on flow through severely stenotic vessels: implications for plaque rupture. J. Biomechanics 33, 443–455.